

Magnon Hall transports on the decorated honeycomb lattice

S. A. Owerre^{1,2}

¹*Perimeter Institute for Theoretical Physics, 31 Caroline St. N., Waterloo, Ontario N2L 2Y5, Canada.*

²*African Institute for Mathematical Sciences, 6 Melrose Road, Muizenberg, Cape Town 7945, South Africa.**

We propose quantum (anti)ferromagnetic insulators on the decorated honeycomb lattice as a realization of magnon Hall transports. In this lattice, a chiral interaction is allowed on the unit cell comprising two coupled triangles. For ferromagnetically coupled triangles, we show that the chiral term generates a staggered and uniform fictitious magnetic flux configurations. In the former, we observe trivial gap in the magnon excitations, hence the chirality-induced Berry curvature vanishes, as well as thermal Hall and spin Nernst conductivities. In the latter, however, we find that magnon excitations are separated from each other and the chirality-induced Berry curvature show peaks at the corners of the Brillouin zone. This leads to nonzero thermal Hall and spin Nernst conductivities. We find that thermal Hall conductivity shows a sign change at fixed magnetic field and varying temperature. For antiferromagnetically coupled triangles, the situation is different, thermal Hall and spin Nernst conductivities change sign as the magnetic field is reversed and vanish at zero field. For fully antiferromagnetic insulator, the system exhibits quantum spin liquid phases. We show that the magnon bulk bands are also gapped and we argue that thermal Hall transports can also be accessible due to nonzero spin chirality.

PACS numbers: 72.20.i, 75.47.-m, 75.30.Ds

Introduction.— Chiral magnons are the new direction for dissipationless transports in quantum magnetic systems, applicable to modern technology such as spintronics and thermal devices [1–6]. In quantum magnets, the spin scalar chirality is defined as the triple product of three neighbouring spin operators $\mathbf{S}_i \cdot (\mathbf{S}_j \times \mathbf{S}_k)$ at sites i, j, k of triangular plaquettes of the lattice. It plays a prominent role in ordered quantum magnets, as well as quantum spin liquids (QSL) as it can be nonzero even in the disordered phase leading to chiral QSL magnetic states. Recently, chirality-induced thermal Hall transports in magnetic systems have attracted considerable attention. Thermal Hall transports in quantum magnets are manifested in the presence of a temperature gradient $-\Delta T$, which transports an induced chiral heat current \mathbf{J}_e [7–9]. The response of the system due to $-\Delta T$ gives rise to transverse thermal Hall conductivity κ_{xy} [7, 9] and transverse spin Nernst conductivity α_{xy}^s [10]. Recent experiments have uncovered chirality-induced magnon Hall transports in a number of three-dimensional (3D) single-layer chiral ferromagnetic pyrochlores — $\text{Lu}_2\text{V}_2\text{O}_7$, $\text{Ho}_2\text{V}_2\text{O}_7$, and $\text{In}_2\text{Mn}_2\text{O}_7$ [8, 11], and in 2D single-layer chiral kagome magnet $\text{Cu}(1-3, \text{bdc})$ [12]. Thermal Hall transport was also observed in the pyrochlore $\text{Tb}_2\text{Ti}_2\text{O}_7$ [13], a material known to host 3D QSL state [14]. A number of interesting features were observed on these chiral magnets. For the pyrochlores, κ_{xy} changes sign upon reversing the direction of magnetic field as the orientations of the spins are reversed. For the kagome magnet, κ_{xy} changes sign as function of magnetic field or temperature [12, 15, 16]. A review of these recent theoretical and experimental developments has been written [17].

Following these fascinating theoretical and experimental results, the author has theoretically proposed a chiral

quantum magnet on the honeycomb lattice [18]. The honeycomb chiral ferromagnetic insulator is analogous to a bosonic version of Haldane model in electronic systems [19]. It has been shown that for this model, κ_{xy} has a fixed sign for all parameter regime [20]. Magnon mediated spin Nernst effect has also been studied using this honeycomb-lattice model [21]. Also recently, we have generalized the chirality-induced magnon transports to bilayer quantum magnets on the honeycomb lattice [22, 23]. In the bilayer honeycomb chiral magnon insulators, the interlayer coupling can be ferromagnetic or antiferromagnetic with strikingly different results. We have shown that ferromagnetic interlayer coupling behaves similarly to single-layer honeycomb insulator with no sign change in κ_{xy} and α_{xy}^s . However, for antiferromagnetic interlayer coupling both κ_{xy} and α_{xy}^s show a sign change as the magnetic field is reversed and κ_{xy} vanishes at zero magnetic field when time-reversal symmetry is preserved. Recently, different authors have studied a limiting case of this model at zero magnetic field [24, 25] and confirmed that, indeed, κ_{xy} vanishes for antiferromagnetic coupling. At the moment, there is no experimental evidence of thermal Hall transports on the honeycomb lattice. However, these fascinating properties of quantum magnets have rekindled a great interest in identifying chiral magnetic systems with nontrivial Hall response.

In this Letter, we study magnon Hall transports of chiral (anti)ferromagnets on the decorated honeycomb lattice. This lattice structure has attracted many investigations. In particular, quantum spin magnets and topological insulators on this lattice show distinctive remarkable features [26–32] different from other systems. It also plays a prominent role in many systems such as the Kitaev model [27] and ultracold atoms [32]. It has also

been synthesized in organic iron acetate quantum magnet [26]. In this lattice, the unit cell contains two coupled triangles and a uniform or staggered Dzyaloshinsky-Moriya (DM) interaction [33] is allowed in the unit cell [30]. We show that the DM interaction induces a fictitious magnetic flux and magnon Hall transports are manifested. Interestingly, the coupling between the triangles can be treated as ferromagnetic or antiferromagnetic with strikingly different magnon Hall transports. In the former, we find that for staggered flux configuration, κ_{xy} and α_{xy}^s vanish, whereas for uniform flux configuration, we find that κ_{xy} and α_{xy}^s are nonzero and κ_{xy} changes sign as a function of temperature. In the latter, both flux configurations have nonzero κ_{xy} and α_{xy}^s . We find that both κ_{xy} and α_{xy}^s change sign as the magnetic field is reversed and both vanish at zero magnetic field in the uniform flux configuration. For fully antiferromagnetic insulator within and between triangles, the ground state is disordered and the magnetic excitations are of interest. We adopt the spinon formalism and show that the magnon bulk bands for different QSL phases are very similar to the chiral ferromagnetic insulators. Thus, thermal Hall response can be measured as a probe of the magnetic excitations in the QSL phases. The proposed phenomena on this lattice are likely to be observed as it is an interpolating lattice between the honeycomb lattice and the kagome lattice.

Model.— The decorated honeycomb lattice is known to possess both magnetically ordered states and QSL states [26, 30]. Specifically, it corresponds to a honeycomb lattice with each site on the hexagon replaced with a triangle as depicted in Fig. 1. We study the chiral ferromagnetic model, which is a magnetically ordered state on the lattice. The Hamiltonian is given by

$$H = - \sum_{\langle ij \rangle} J_{ij} \mathbf{S}_i \cdot \mathbf{S}_j + \sum_{\langle ij \rangle} \mathbf{D}_{ij} \cdot \mathbf{S}_i \times \mathbf{S}_j - h \sum_i S_i^z, \quad (1)$$

where $J_{ij} > 0$ are the ferromagnetic couplings within sites on the triangles “ Δ ” and between triangles “ $\Delta \rightarrow \Delta$ ” as shown in Fig. 1, and \mathbf{D}_{ij} are the DM interaction vectors between site i and j , which are allowed by the triangular plaquettes in the unit cell shown in Fig. 2. We assume a DM interaction along the direction of the magnetic field, i.e. $\mathbf{D}_{ij} = D\hat{\mathbf{z}}$, where D is the magnitude of the DM interaction, and h is the magnetic field in units of $g\mu_B$. It should be noted that Eq. 1 remains ferromagnetic despite the DM interaction as in other chiral ferromagnetic insulators. There two ferromagnetic ordered states in decorated honeycomb lattice. The first case corresponds to $J > 0$ and $J' > 0$, i.e. fully polarized ferromagnets on sublattice A (up pointing triangles) and B (down pointing triangles). The second case corresponds to $J > 0$ and $J' < 0$, i.e., antiferromagnetic interaction between triangles. In this case, the spins on sublattice A point in opposite direction to those on sublattice B .

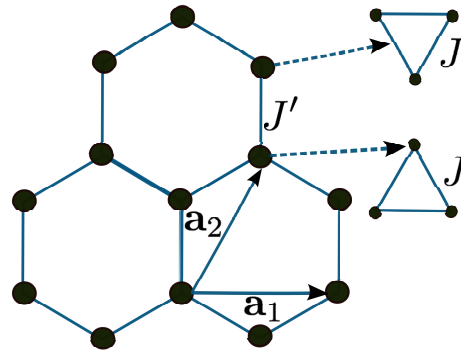


FIG. 1. Color online. Schematics of decorated honeycomb lattice. We assume isotropic interaction J within triangles and isotropic interaction J' between triangles. The lattice basis vectors are chosen as $\mathbf{a}_1 = 2\hat{\mathbf{x}}$ and $\mathbf{a}_2 = \hat{\mathbf{x}} + \sqrt{3}\hat{\mathbf{y}}$.

Band structure.— We are interested in the low-temperature regime of the ordered chiral magnets. In this low-temperature regime, only few magnons are thermal excited, hence the linearized Holstein-Primakoff boson representation [34] is valid. The magnon tight binding model for the first case discussed above ($J, J' > 0$) is given by

$$H_B = v_0 \sum_{j;\Delta;\Delta \rightarrow \Delta} n_j - v'_s \sum_{\langle ij \rangle;\Delta \rightarrow \Delta} (b_i^\dagger b_j + h.c.) \quad (2)$$

$$- v_t \sum_{\langle ij \rangle;\Delta} (e^{i\phi_{ij}} b_i^\dagger b_j + h.c.)$$

where $n_j = b_j^\dagger b_j$, $v_0 = 2v_s + v'_s + h$, $v_t = \sqrt{v_s^2 + v_D^2} = JS/\cos(\phi_{ij})$, $v_s(v'_s)(v_D) = JS(J'S)(DS)$; $\phi_{ij} = \pm\phi = \arctan(D/J)$ is a magnetic flux generated by the DM interaction within the triangular plaquettes, similar to Haldane model [19]. The configurations of ϕ_{ij} are depicted in Fig. 2. The total flux in the dodecagon consisting of twelve sites is 2ϕ and 0 respectively. We assume that ϕ_{ij} vanishes between triangles. The momentum space Hamiltonian can be written as $H_B = \sum_{\mathbf{k}} \Psi_{\mathbf{k}}^\dagger \cdot \mathcal{H}(\mathbf{k}) \cdot \Psi_{\mathbf{k}}$, with $\Psi_{\mathbf{k}}^\dagger = (a_{\mu,\mathbf{k}}^\dagger, b_{\nu,\mathbf{k}}^\dagger)$, where $\mu = 1, 2, 3$ and $\nu = 4, 5, 6$. The Bogoliubov Hamiltonian $\mathcal{H}(\mathbf{k})$ is Hermitian and depends on the flux configurations.

In the following, we take J as the unit of energy. An example of the band structure for two different configurations is shown in Fig. 3. For the pristine model $\phi = 0$ or π , the magnon band structure has four dispersive bands and two flat bands. In the former, the bands exhibit Dirac points at the corners of the Brillouin zone $\pm\mathbf{K} = (\pm 2\pi/3, 0)$ and there exist two quadratic band touching points at $\mathbf{\Gamma} = (0, 0)$. In the presence of the DM interaction ($\phi \neq 0, \pi$), the flat bands become dispersive and the degeneracies of the Dirac nodes at $\pm\mathbf{K}$ and $\mathbf{\Gamma}$ are lifted for the uniform flux configuration as shown in Fig. 3(a). For the staggered configuration, however, band-touching points between neighbouring bands

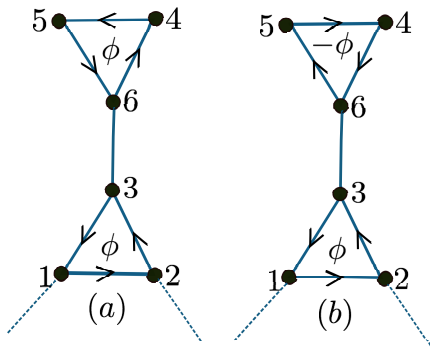


FIG. 2. Two possible configurations of ϕ_{ij} on the decorated honeycomb lattice unit cell. (a) Uniform. (b) Staggered. The arrows indicate the sign of the fictitious magnetic flux.

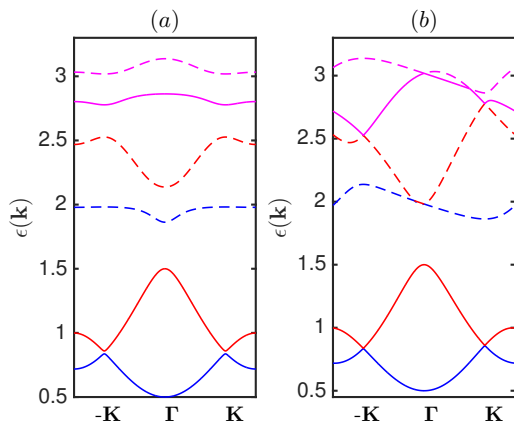


FIG. 3. Color online. The band structure of the chiral ferromagnet on the decorated honeycomb lattice for $J = J' = 1$, $h = 0.5$, $\phi = 0.05\pi$. The labels (a) and (b) correspond to two different flux configuration in Fig. 2. The gap of the lowest band at Γ is h .

always exit in the spectrum, thus the system remains metallic. It is noted that for $J' = 0$, the band structure does not necessarily reduce to those of kagome lattice as one might expect. In this case, the band structure has only three flat bands in contrast to the kagome lattice [7].

For the second case ($J > 0, J' < 0$), we perform a π -rotation about the S_x -axis on sublattice B , given by the transformation $S_{i,j}^x \rightarrow S_{i,j}^x$, $S_{i,j}^y \rightarrow -S_{i,j}^y$, $S_{i,j}^z \rightarrow -S_{i,j}^z$, which flips the sign of the DM interaction and the magnetic field on sublattice B . The magnon tight binding Hamiltonian is given by

$$H_B = \tilde{v}_0 \sum_{j;\Delta;\Delta \rightarrow \Delta} n_j + |v'_s| \sum_{\langle ij \rangle; \Delta \rightarrow \Delta} (b_i^\dagger b_j + h.c.) \quad (3)$$

$$- v_t \sum_{\langle ij \rangle; \tau} (e^{i\tau\phi_{ij}} b_i^\dagger b_j + h.c.) + h \sum_{j;\tau} \tau n_j$$

where $\tau = \pm$ for Δ and ∇ respectively, $\tilde{v}_0 = 2v_s - |v'_s|$. The band structure is depicted in Fig. 4 and shows sig-

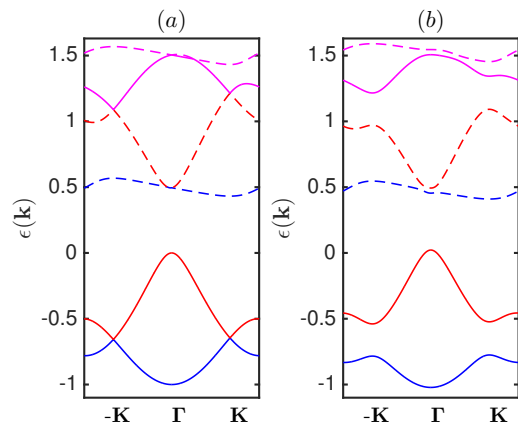


FIG. 4. Color online. The band structure of the chiral ferromagnet with antiferromagnetic coupling between triangles for $J = |J'| = 1$, $\phi = 0.025\pi$: (a) $h = 0$ and (b) $h = 0.15$, in the uniform flux configuration depicted above.

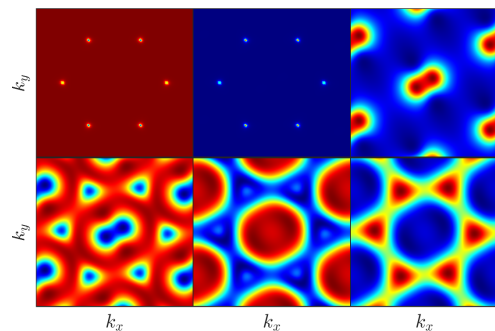


FIG. 5. Color online. Berry curvatures of the bands in Fig. 3 (a) in ascending order from left to right. The peaks occur at the corners and center of the Brillouin zone.

nificant differences from the ferromagnetically coupled triangles. In this case, the uniform and staggered (not shown) flux configurations show gapped magnon bands. As shown in Fig. 4, the nontrivial gaps between neighbouring bands are induced by the staggered magnetic field in contrast to ferromagnetically coupled triangles.

Magnon Hall transports.—Theoretically, thermal Hall response in chiral quantum magnets can be understood in terms of the chirality-induced Berry curvatures. This leads to dissipationless magnon edge states. Needless to say, chiral edge states exist in the present model [28]. In a longitudinal temperature gradient, the magnon edge states carry a transverse heat (spin) current. Let us first consider ferromagnetic couplings within and between triangles, that is $J, J' > 0$. Using linear response theory, one can derive the response of the system to a longitudinal temperature gradient which gives [9] $\kappa_{xy} = -2k_B^2 T V^{-1} \sum_{\mathbf{k}\mu} c_2(n_\mu) \Omega_\mu(\mathbf{k})$, where V is the volume of the system, k_B is the Boltzmann constant,

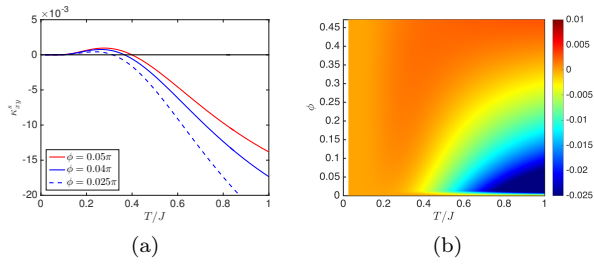


FIG. 6. Color online. (a). κ_{xy} vs. T/J for several values of uniform ϕ configuration and fixed values of $J' = 1$, $h = 0.5$. (b) The contour plot of κ_{xy} in the T/J - ϕ plane.

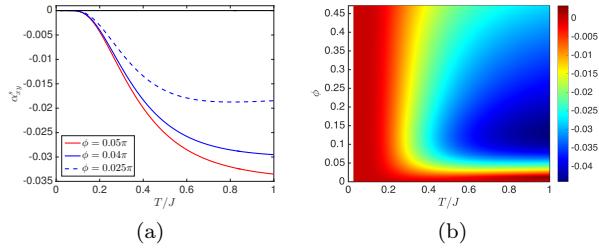


FIG. 7. Color online. (a). α_{xy}^s vs. T/J for several values of uniform ϕ configuration and fixed values of $J' = 1$, $h = 0.5$. (b) The contour plot of α_{xy}^s in the T/J - ϕ plane.

T is the temperature, $n_\mu \equiv n_B[\epsilon_\mu(\mathbf{k})] = [e^{\epsilon_\mu(\mathbf{k})/k_B T} - 1]^{-1}$ is the Bose function, $c_2(x) = (1+x)(\ln \frac{1+x}{x})^2 - (\ln x)^2 - 2\text{Li}_2(-x)$, $\text{Li}_2(x)$ is a dilogarithm. Similarly, $\alpha_{xy}^s = k_B V^{-1} \sum_{\mathbf{k}\mu} c_1(n_\mu) \Omega_\mu(\mathbf{k})$, [10] where $c_1(x) = (1+x) \ln(1+x) - x \ln x$.

Evidently, the chirality-induced Berry curvature is the main component in these expressions. It is defined as $\Omega_\mu(\mathbf{k}) = \nabla_{\mathbf{k}} \times \mathcal{A}_\mu(\mathbf{k})$, where $\mathcal{A}_\mu(\mathbf{k}) = i \langle \psi_\mu(\mathbf{k}) | \nabla_{\mathbf{k}} | \psi_\mu(\mathbf{k}) \rangle$ is a vector potential generated by the DM interaction, μ labels the energy bands and $\psi_\mu(\mathbf{k})$ are the eigenstates of the magnon Hamiltonian. An example of the Berry curvatures is shown in Fig 5. The peaks occur at the avoided energy crossings at the corners of the Brillouin

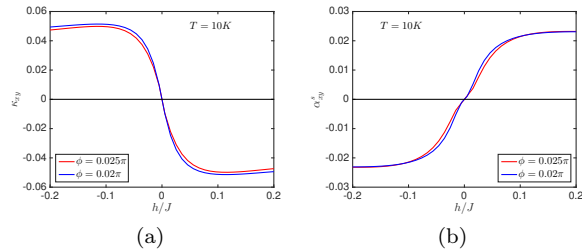


FIG. 8. Color online. (a). κ_{xy} vs. h for antiferromagnetic coupling between triangles. (b) α_{xy}^s vs. h for antiferromagnetic coupling between triangles. The uniform flux configuration is assumed and $J' = 1$.

zone. We have also shown the plot of κ_{xy} and α_{xy}^s as function of temperature in Figs. 6 and 7. We see that κ_{xy} changes sign as the temperature varies, whereas α_{xy}^s does not. The signs of κ_{xy} and α_{xy}^s are fixed for reversed magnetic field and nonzero at zero magnetic field. In contrast, for antiferromagnetic couplings between triangles, we consider only the positive energies and find that κ_{xy} and α_{xy}^s change sign as the magnetic field is reversed and vanish at $h = 0$ as shown in Fig. 8. The change of sign with reversed magnetic field occur with the uniform configuration and it is inherited from the Berry curvature: $\Omega_\mu(\mathbf{k}) \rightarrow -\Omega_\mu(\mathbf{k})$ as $h \rightarrow -h$. It can also be understood from the magnon band structure and propagation of magnon edge states. In particular, the vanishing κ_{xy} and α_{xy}^s at $h = 0$ is evident from the metallic nature of the band structure in Fig. 4 (a).

Quantum spin liquid regime.— The decorated honeycomb lattice is also known to possess disordered and QSL phases [26, 30]. Quantum disordered ground state is only present in the antiferromagnetic model $H_A = \sum_{\langle ij \rangle} J_{ij} \mathbf{S}_i \cdot \mathbf{S}_j$, $J_{ij} > 0$, as it is impossible to satisfy concurrent antiferromagnetic interaction at the vertices of the triangles. As recently reported on the pyrochlore $\text{Tb}_2\text{Ti}_2\text{O}_7$ [13], thermal Hall transport measurement can be used to probe the excitations of disordered quantum systems. Theoretically, it is usually convenient to adopt the spinon formalism, which is valid in the disordered phase. In the spinon formalism, we write $\mathbf{S}_i = \frac{1}{2} \sum_{\sigma, \sigma'} b_{i, \sigma}^\dagger \boldsymbol{\sigma}_{\sigma, \sigma'} b_{i, \sigma'}$, where $b_{i, \sigma}^\dagger$ ($b_{i, \sigma}$) represent bosonic or fermionic creation (annihilation) operators, subject to the constraint $\sum_{\sigma} b_{i, \sigma}^\dagger b_{i, \sigma} = 1$; $\sigma, \sigma' = \uparrow, \downarrow$ and $\boldsymbol{\sigma}$ is the triplet Pauli matrices. The mean-field Hamiltonian of H_A is given by

$$H_{MF} = - \sum_{\langle ij \rangle, \sigma} J_{ij} (b_{i, \sigma}^\dagger b_{j, \sigma} \chi_{ij}^* + h.c.) + \sum_{\langle ij \rangle} J_{ij} |\chi_{ij}|^2 + \sum_{i, \sigma} \lambda_i (b_{i, \sigma}^\dagger b_{i, \sigma} - 1), \quad (4)$$

where $\chi_{ij} = \frac{1}{2} \sum_{\sigma} \langle b_{i, \sigma}^\dagger b_{j, \sigma} \rangle$ is the resonating valence bond order parameter and $\lambda_i = \lambda$ is the Lagrange multiplier. The chirality-induced fictitious magnetic flux can be taken into consideration by selecting a mean-field Ansatz given by $\bar{\chi}_{ij} = |\chi_{ij}| e^{\phi_{ij}}$, where ϕ_{ij} has the configurations defined above. Also, one can select two different bond representations within and between the triangles, $|\chi_{ij}| = \chi J$ and $|\chi_{ij}| = \chi J'$ respectively. The band structure is obtained from the self-consistent bond operator mean-field theory. As shown in Ref. [30], there are several gap phases in the magnon bulk bands. In fact, the band structure is very similar to those of ferromagnetic insulators studied above. This suggests that magnon Hall transports are possible in the QSL regimes.

Conclusion.— We have proposed quantum magnetic insulators on the decorated honeycomb lattice as a candidate for magnon mediated Hall transports in quantum

magnets. For chiral ferromagnetic insulators on this lattice, we show that the magnetic excitations exhibit non-trivial topology with nonvanishing Berry curvature in the uniform and staggered flux configurations. The system realizes thermal Hall effect as well as spin Nernst effect. We show that for ferromagnetically coupled triangles in the unit cell, thermal Hall conductivity changes sign as function of temperature, whereas spin Nernst conductivity has a fixed sign. For antiferromagnetically coupled triangles, we show that both conductivities change sign as the magnetic field is reversed and vanish at zero field. We also show that frustrated antiferromagnetic model on this lattice exhibits similar features. Thus, magnon Hall transports can be accessed both in the ordered regime and the quantum spin liquid regimes of the decorated honeycomb lattice.

Acknowledgments.— Research at Perimeter Institute is supported by the Government of Canada through Industry Canada and by the Province of Ontario through the Ministry of Research and Innovation.

* solomon@aims.ac.za

- [1] V. V. Kruglyak, S. O. Demokritov, and D. Grundler, J. Phys. D: Appl. Phys. **43**, 264001 (2010).
- [2] B. Lenk, *et al*, Physics Reports **507**, 107 (2011).
- [3] A. V. Chumak, *et al*, Nature Physics **11**, 453 (2015).
- [4] R. Shindou *et al.*, Phys. Rev. B **87**, 174427 (2013); Phys. Rev. B **87**, 174402 (2013).
- [5] R. Matsumoto, R. Shindou, and S. Murakami, Phys. Rev. B **89**, 054420 (2014).
- [6] L. Zhang, J. Ren, J. S. Wang, and B. Li, Phys. Rev. B **87**, 144101 (2013).
- [7] H. Katsura, N. Nagaosa, and P. A. Lee Phys. Rev. Lett. **104**, 066403 (2010).
- [8] S. Y. Onose *et al* Science **329**, 297 (2010).
- [9] R. Matsumoto and S. Murakami Phys. Rev. Lett. **106**, 197202 (2011); Phys. Rev. B **84**, 184406 (2011).
- [10] A. A. Kovalev and V. Zyuzin, Phys. Rev. B **93**, 161106(R) (2016).
- [11] T. Ideue *et al.*, Phys. Rev. Lett. **85**, 134411 (2012).
- [12] M. Hirschberger *et al* Phys. Rev. Lett. **115**, 106603 (2015).
- [13] M. Hirschberger, J. W. Krizan, R. J. Cava, and N. P. Ong, Science **348**, 106 (2015).
- [14] Hamid R. Molavian, Michel J. P. Gingras and B. Canals, Phys. Rev. Lett. **98**, 157204 (2007); L. Balents, Nature **464**, 199-208 (2010); M. J. P. Gingras and P. A. McClarty, Rep. Prog. Phys. **77** 056501 (2014).
- [15] H. Lee, J. H. Han, and P. A. Lee Phys. Rev. Lett. **91**,125413 (2015).
- [16] A. Mook, J. Henk, and I. Mertig Phys. Rev. B **90**, 024412 (2014); A. Mook, J. Henk, and I. Mertig, Phys. Rev. B **89**, 134409 (2014).
- [17] J. H. Han, H. Lee, arXiv:1604.08290
- [18] S. A. Owerre, arXiv:1602.06772.
- [19] F. D. M. Haldane Phys. Rev. B **61**, 2015 (1988).
- [20] S. A. Owerre, arXiv:1603.04331.
- [21] S. K. Kim *et al.*, arXiv:1603.04827.
- [22] S. A. Owerre, arXiv:1604.05292.
- [23] S. A. Owerre, arXiv:1605.07971.
- [24] R. Cheng, S. Okamoto, D. Xiao, arXiv:1606.01952.
- [25] V. Zyuzin and A. A. Kovalev, arXiv:1606.03088.
- [26] Y.-Z. Zheng *et al*, Angew. Chem., Int. Ed. **46**, 6076 (2007).
- [27] H. Yao and S. A. Kivelson, Phys. Rev. Lett. **99**, 247203 (2007).
- [28] A. Rüegg, J. Wen, and G. A. Fiete, Phys. Rev. B **81**, 205115 (2010).
- [29] J. O. Fjaerestad, arXiv:0811.3789.
- [30] B.-J. Yang, A. Paramakanti, and Y. B. Kim, Phys. Rev. B **81**, 134418 (2010).
- [31] W. -C. Chen *et al*, Phys. Rev. B **86**, 085311 (2012).
- [32] H. -F. Lin *et al*, Phys. Rev. A **90**, 053627 (2014).
- [33] I. Dzyaloshinsky J. Phys. Chem. Solids **4**, 241 1958; T. Moriya Phys. Rev. **120**, 91 (1960).
- [34] T. Holstein and H. Primakoff, Phys. Rev. **58**, 1098 (1940).